Multi-Task Learning as a Step Toward Building General-Purpose Hydrological Forecasting Systems

Bekir Z. Demiray^{1,2,*}, Ibrahim Demir^{3,4}

- ¹ IIHR—Hydroscience and Engineering, University of Iowa, Iowa City, Iowa, USA
- ² Interdisciplinary Graduate Program in Informatics, University of Iowa, Iowa City, Iowa, USA
- ³ River-Coastal Science and Engineering, Tulane University, New Orleans, LA, USA
- ⁴ ByWater Institute, Tulane University, New Orleans, LA, USA
- * Corresponding Author, Email: bekirzahit-demiray@uiowa.edu

Abstract

Streamflow and soil moisture are two critical variables in the hydrological cycle, linked through infiltration, runoff generation, and groundwater recharge. Traditional forecasting approaches often treat them independently, overlooking interdependencies and limiting predictive skill. This study investigates Multi-Task Learning (MTL) for daily prediction of both variables using the CAMELS dataset derived from the CARAVAN archive. Two task-aware architectures—a Transformer-based and a Mamba-based model—were developed, where shared representations are combined with task identifiers to distinguish outputs for streamflow and soil moisture. Both models were trained to produce 7-day forecasts with balanced sampling across tasks. Results across more than 600 U.S. basins show that MTL models achieve accuracy comparable to or slightly better than single-task baselines, demonstrating the feasibility of learning shared representations. By confirming that one model can distinguish between processes and predict multiple targets without loss of skill, this study establishes a proof of concept for unified, multivariable forecasting systems.

Keywords

Multi-Task Learning (MTL), Transformer, State-Space Models (Mamba), Hydrology, Streamflow, Soil Moisture, Explainable AI (SHAP), Deep Learning

This manuscript is an EarthArXiv preprint and has been submitted for possible publication in a peer reviewed journal. Please note that this has not been peer-reviewed before and is currently undergoing peer review for the first time. Subsequent versions of this manuscript may have slightly different content.

1. Introduction

Continuous and accurate forecasting of the Earth's water cycle is essential for protecting populations, ecosystems, and economies. As fundamental components of this cycle, streamflow and soil moisture serve as key indicators of water availability and climate-related hazards (Tanir et al., 2024). Streamflow, which represents the total water draining from a landscape, is directly linked to both floods and droughts. Excessively high flows pose significant risks to infrastructure and human life globally (Ward et al., 2013; Alabbad et al., 2023), while sustained low flows can signal impending drought, straining municipal water supplies, reducing agricultural output, and limiting hydropower generation (Mishra & Singh, 2010).

Soil moisture is equally vital, underpinning ecosystem health, agricultural productivity, and land–atmosphere interactions. Deficits in soil moisture are primary indicators of agricultural drought, while its spatial and temporal variability influences evapotranspiration, groundwater recharge, and vegetation resilience (Islam et al., 2025). Importantly, the degree of soil saturation regulates how much rainfall infiltrates versus how much becomes runoff, thereby controlling the severity of floods (Seneviratne et al., 2010). For example, antecedent soil moisture has been shown to amplify peak flows during heavy precipitation events (Seo et al., 2019), emphasizing its role as a dominant flood precursor (Ye et al., 2021; Webb et al., 2025). Conversely, soil moisture dynamics can be shaped by streamflow variability through processes such as overbank flooding and groundwater–river exchanges.

The urgency of improving forecasts for these variables is underscored by the increasing frequency and severity of natural disasters worldwide. Climate change is intensifying extreme weather events and altering precipitation patterns, thereby exacerbating both flood and drought risks (WMO, 2021; IPCC, 2023; UNESCO, 2023). Flooding, in particular, remains the most widespread natural hazard, producing devastating economic losses and human casualties (Davenport et al., 2021; Tabari, 2020; NOAA, 2022; Cikmaz et al., 2025). Limited focus on coupled dynamics of soil moisture and streamflow risks underestimating the magnitude of such hazards. Developing integrated forecasting frameworks that capture their interactions is thus a scientific priority and a societal necessity for climate resilience and disaster preparedness (IPCC, 2021).

Over the past decade, the domain has evolved from early neural networks—perceptrons and multilayer nets trained by backpropagation (Bayar et al., 2009) —to modern deep learning models (Xiang et al., 2021) that harness large spatiotemporal environmental data through modern sensor networks (Demir et al., 2015) to improve hydrological forecasting. Long Short-Term Memory (LSTM) networks were among the first architectures to demonstrate broad success, showing strong performance across diverse hydroclimatic regions (Kratzert et al., 2019; Xiang et al., 2020; Sit et al., 2022). Kratzert et al. (2019) demonstrated that LSTM networks trained across multiple basins can outperform traditional hydrological models and capture complex catchment behaviors (e.g. snow dynamics) without explicit physical parameterization. Arsenault et al. (2023) further validated LSTM's superiority over conventional methods in ungauged basins across northeastern North America. The rise of Transformer-based architecture has further

advanced streamflow forecasting (Castangia et al., 2023; Demiray and Demir, 2024; Koya and Roy, 2024).

Castangia et al. (2023) reported superior flood prediction performance using Transformers in the Sava River Basin, while Koya and Roy (2024) conducted single-basin training experiments with the Temporal Fusion Transformer across more than 2,600 basins, demonstrating that the architecture consistently outperformed recurrent networks and provided improved interpretability at the basin scale. Hybrid approaches have also shown promise in advancing streamflow forecasting (Khandelwal et al., 2020; Zuo et al., 2020; Fang et al., 2024). For example, Zuo et al. (2020) combined variational mode decomposition with LSTMs to improve runoff forecasting, while Fang et al. (2024) developed a decomposition—Transformer ensemble to enhance multistep predictions. Beyond these examples, many other works have explored diverse strategies, ranging from graph neural networks (Liu et al., 2022a; Sun et al., 2021; Xiang and Demir, 2022) to recurrent variants such as GRUs (Wang et al., 2020; Le et al., 2021) and more recent statespace architectures like Mamba (Jia et al., 2024; Demiray and Demir, 2025), each contributing to improved skill in streamflow prediction.

This growing body of literature demonstrates both the flexibility and rapid progress of deep learning in hydrology. Several review articles provide comprehensive syntheses of these developments (Sit et al., 2020; Sit et al., 2022; Ng et al., 2023; Zhao et al., 2024), underscoring that deep learning has become a central paradigm for streamflow forecasting, with an expanding range of architectures and methodological innovations.

Deep learning has become an increasingly powerful approach for soil moisture prediction, as synthesized by recent reviews that evaluates modern architectures and workflows with benchmark datasets (Wang et al., 2024; Abbes et al., 2024; Senanayake et al., 2024; Demir et al., 2022). When paired with large-scale observational products—particularly satellite missions such as SMAP and ASCAT and modern reanalysis—deep networks can exploit rich spatiotemporal information to improve skill across regions and depths (Gao et al., 2022; Liu et al., 2022b). Recurrent and convolutional architectures, in particular, have been widely applied, demonstrating strong capability in capturing short-term variability and longer-term dependencies in soil water processes (ElSaadani et al., 2021; Wang et al., 2024). Beyond standard LSTM/ConvLSTM designs, specialized recurrent variants have been proposed to better encode temporal causality, attention, and lag dependencies.

For example, Li et al. (2022) developed a causality-structured LSTM that improved multiday forecasts across diverse environments, while Zhang et al. (2022) used a CNN–LSTM hybrid to construct the SGD-SM 2.0 dataset, a seamless global daily soil moisture record from 2002–2022. Rabiei et al. (2025) showed that ConvLSTM architectures combined with SMAP and SOLUS100 data improve both surface and subsurface soil moisture estimation. Hybrid and advanced approaches are also gaining momentum. Xi et al. (2025) developed a physics-guided deep learning (PGDL) framework that integrated the terrestrial ecosystem model with LSTMs to improve predictive skill while preserving interpretability. More recently, a self-supervised Transformer-based model has been proposed to improve generalization under unseen

meteorological and soil depth conditions, outperforming LSTMs in capturing extremes such as droughts (Wang et al., 2025). Collectively, these studies demonstrate significant progress toward models that are scalable, interpretable, and generalizable across diverse hydroclimatic conditions.

Multi-Task Learning (MTL) is a machine learning paradigm in which a single model is trained to solve multiple related tasks simultaneously by sharing internal representations (Caruana, 1997; Ruder, 2017). By leveraging commonalities in the data, MTL has shown benefits in efficiency, generalization, and robustness across domains such as computer vision, speech recognition, and natural language processing (Bommasani, 2021; Lu et al., 2022; Barrault et al., 2022; Xiao et al., 2024). In particular, large language models illustrate the promise of this approach: trained on diverse objectives with task identifiers or prompts, they perform a wide spectrum of tasks within a single architecture (Brown et al., 2020; Wei et al., 2021; Wei et al., 2022; Touvron et al., 2023; Team et al., 2023). This paradigm shift highlights the potential of unifying related predictive problems without the need for bespoke models for each task. While MTL has been transformative in other domains, its application in hydrology is still emerging. Sadler et al. (2022) jointly predicted daily streamflow and water temperature across 101 U.S. sites, demonstrating improved accuracy compared to single-task models by exploiting interdependencies between variables.

Similarly, Hu et al. (2024) used stacked LSTMs to simulate streamflow and multiple water quality parameters, while Li et al. (2023) integrated CNN and LSTM architectures to predict runoff and actual evapotranspiration in the Tibetan Plateau, underscoring the value of spatial information. Ouyang et al. (2023) further demonstrated "variable synergy," where a model trained on streamflow and evapotranspiration improved non-target predictions such as soil moisture. Other studies have adopted broader interpretations of MTL. Tran and Kim (2024) treated different lead times at a single site as separate tasks, while Lu et al. (2023) combined GCNs with LSTMs for runoff prediction and flow calibration, reporting gains primarily for runoff. Huang et al. (2023) framed seasonal water level forecasting as a multi-task problem by assigning distinct tasks to different seasons. Collectively, these studies highlight both the potential and the unsettled boundaries of multi-task learning in hydrology, particularly in relation to streamflow, reinforcing the need for foundational explorations in this area.

Crucially, the significance of applying MTL in hydrology does not hinge only on surpassing single-task baselines in terms of predictive accuracy. Rather, its value lies in establishing whether a single model can simultaneously represent and differentiate multiple hydrological processes when guided by identical inputs and explicit task identifiers. Unlike prior work that often introduces specialized architectures for each additional target variable, our approach explores a streamlined alternative: encoding task identity directly through embeddings while maintaining a common representational backbone. This design tests whether hydrological tasks can be learned within a unified framework without manual architectural separation, offering a scalable path toward multi-purpose forecasting systems.

In this study, we present one of the first systematic applications of an embedding-based multi-task learning (MTL) framework to support the prediction of both streamflow and soil moisture. These two variables were selected for their relevance to flood and drought risk, as well as their underlying connections within the hydrological cycle. Data from 628 stations is used from the CAMELS dataset, accessed via the CARAVAN platform (Kratzert et al., 2023). A seven-day prediction horizon is adopted, and performance is evaluated using eleven hydrological metrics, including NSE and KGE. Two multi-task model architectures are developed—one based on Transformer and the other on Mamba—and compared against single-task models and recurrent baselines such as LSTM and GRU. To interpret model behavior, SHAP-based explainability is applied to identify the most influential input features for each task.

The broader objective of the study is to establish a foundation for incrementally expanding to additional targets—such as evapotranspiration, water temperature, or rainfall downscaling—within a single system. By aligning with broader trends in machine learning toward general-purpose models, this study aims to position hydrology to move beyond siloed, task-specific forecasting pipelines and toward integrated AI frameworks capable of learning multiple processes simultaneously.

This paper is organized as follows. Section 2 introduces the study area and describes the dataset used in this research, then outlines the methodological framework, including model architectures, training procedures, and evaluation metrics. Section 3 presents the experimental results alongside a detailed analysis and discussion. Finally, Section 4 summarizes the main conclusions and highlights potential directions for future research.

2. Methods

The objective of this study is to evaluate whether multi-task learning (MTL) can provide a unified framework for hydrological forecasting by enabling a single model to learn both streamflow and soil moisture prediction tasks. Unlike multivariate prediction, where multiple variables are predicted simultaneously, our formulation treats each variable as a distinct task. Inputs to the model are identical across tasks, and a task identifier is provided to specify whether the model should generate streamflow or soil moisture predictions. This design allows us to test whether task identity can be encoded through embeddings, enabling a shared model backbone to flexibly represent multiple hydrological processes. To investigate this, we compare two multitask architectures—one based on a Transformer encoder and the other on a state-space Mamba network—against their single-task counterparts and recurrent baselines (LSTM and GRU). This section first provides the information about the study area and dataset, then outlines compared architectures and training setup, followed by the metrics used to evaluate predictive skill.

2.1. Study Area and Dataset

This study employs the CARAVAN dataset (Kratzert et al., 2023), an open-source large-sample hydrological dataset that harmonizes multiple regional CAMELS-type datasets (Addor et al., 2017; Alvarez-Garreton et al., 2018; Coxon et al., 2020; Fowler et al., 2021), along with

HYSETS (Arsenault et al., 2020) and LamaH-CE (Klingler et al., 2021). CARAVAN provides basin-scale daily streamflow records, meteorological forcings, and static catchment attributes for more than 6,800 basins worldwide, covering a broad range of climatic and physiographic conditions. Meteorological forcings are derived from ERA5-Land reanalysis (Muñoz-Sabater et al., 2021), while static attributes are aggregated from HydroATLAS (Lehner et al., 2019; Linke et al., 2019), enabling consistent large-sample analyses across regions.

Using CAMELS-US within the CARAVAN dataset, we have curated a subset of 628 basins based on strict data quality and temporal availability criteria. Specifically, basins with more than 30 consecutive days of missing data were excluded to ensure reliability. For the remaining basins, shorter gaps were filled via linear interpolation. Additionally, each selected basin was required to include at least 15 years of training data (1980–2002), 2 years of validation data (2003–2007), and 3 years of testing data (2008–2016). This ensured a minimum of 20 years of continuous observations per basin, providing robust temporal coverage for model development and evaluation. Figure 1 shows the geographic distribution of the selected basins, highlighting the diverse hydroclimatic settings included in this study.

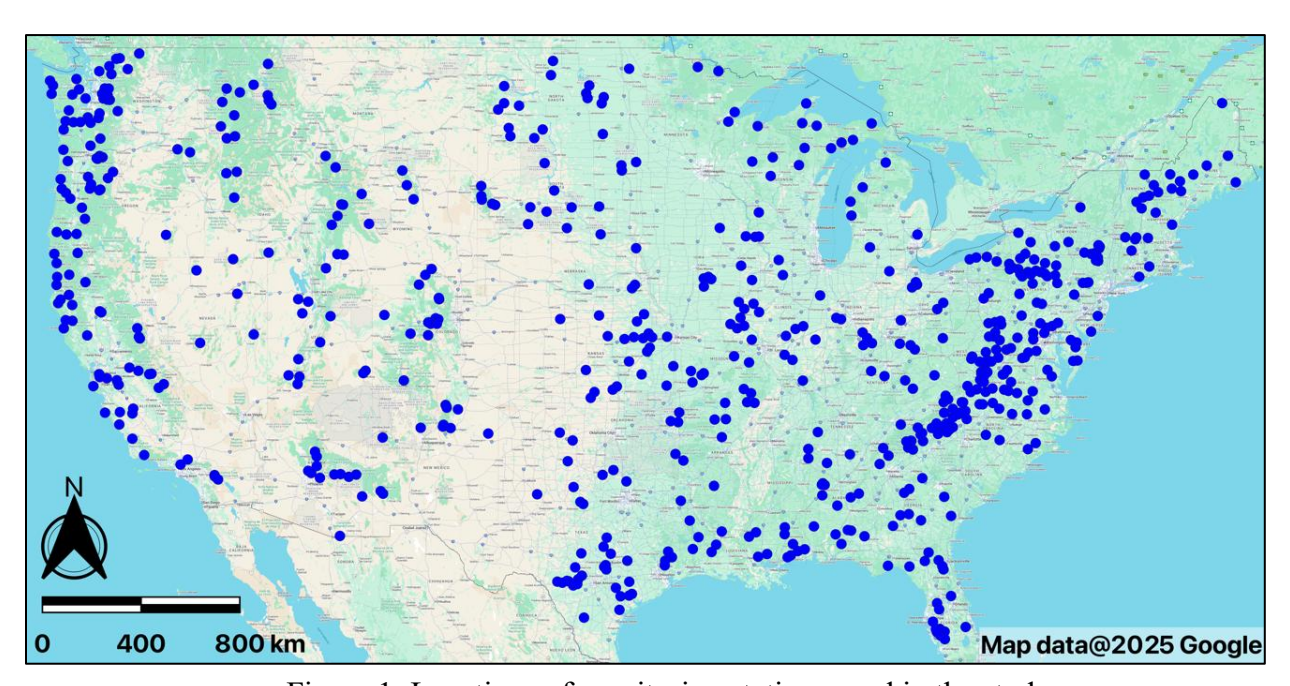


Figure 1: Locations of monitoring stations used in the study

The final dataset consists of 41 continuous time-series variables and 211 static attributes describing physiographic, climatic, and anthropogenic catchment characteristics. All continuous variables were standardized using a z-score transformation, with mean and variance calculated from the training period only to prevent information leakage into validation and testing phases. In addition to streamflow, soil moisture was a primary prediction target. CARAVAN provides soil moisture at four depths; to capture integrated dynamics, we derived a new feature by averaging across depths to obtain a basin-level soil moisture index. This aggregated target was

predicted alongside streamflow in our multi-task learning experiments, while the original depthresolved variables were retained as input features to preserve vertical information. A complete list of the time-series and static predictors used in this study is provided in the Supplementary Material (Tables S1–S2).

2.2. Model Comparison and Evaluation

2.2.1. LSTM and GRU Models

Long Short-Term Memory (LSTM) networks (Hochreiter & Schmidhuber, 1997) and Gated Recurrent Units (GRUs; Cho et al., 2014) are recurrent neural network (RNN) variants specifically designed to capture long-term dependencies in sequential data. Unlike classical RNNs, which suffer from vanishing and exploding gradients, LSTMs and GRUs employ gating mechanisms that regulate the flow of information, enabling them to learn nonlinear lagged responses across extended sequences. This ability is particularly important in hydrology, where processes such as soil moisture memory, snow accumulation and melting, and groundwater recharge exert delayed but critical influences on streamflow and water balance.

The LSTM introduces a dedicated memory cell with input, forget, and output gates, allowing the network to selectively retain or discard information at each time step. In contrast, GRUs simplify the design by combining the input and forget gates into an update gate, while also using a reset gate to control information flow. This streamlined structure reduces the number of parameters, making GRUs computationally more efficient while often achieving performance comparable to LSTMs (Chung et al., 2014).

In hydrological modeling, both architectures have become widely adopted as baseline models. Numerous studies have demonstrated their ability to outperform traditional conceptual or physically based models by learning complex relationships directly from data, particularly in large-sample streamflow prediction tasks (Kratzert et al., 2019; Le et al., 2021; Arsenault et al., 2023). Subsequent reviews have consolidated these findings, identifying recurrent neural networks as among the most robust and consistently successful architectures in hydrological machine learning (Sit et al., 2020; Sit et al., 2022; Ng et al., 2023; Zhao et al., 2024).

In this study, the LSTM benchmark configuration follows the widely adopted setup proposed by Kratzert et al. (2021), which has also been employed in subsequent hydrological studies such as Liu et al. (2024). Specifically, the network employs a sequence length of 365 days to incorporate seasonal cycles, a hidden size of 256 units, and a dropout rate of 0.4 for regularization. This setup draws on commonly adopted practices in hydrological deep learning, offering a rigorous baseline for evaluating newer models. GRU benchmark is implemented with the same architecture and hyperparameters, differing only in the replacement of LSTM cells with GRU units. This parallel design allows for a controlled comparison of recurrent cell choice while holding other modeling aspects constant. By including both LSTM and GRU as baseline models, this study ensures that the performance of embedding-based multi-task frameworks can be meaningfully contextualized against benchmark recurrent methods that have proven effective for streamflow and soil moisture prediction in prior studies.

2.2.2. Transformer Model

The Transformer architecture, originally introduced by Vaswani et al. (2017), marked a departure from recurrent designs by relying entirely on self-attention mechanisms to model sequential dependencies. Instead of propagating information step by step through time as in RNNs, the Transformer encodes the entire sequence in parallel, learning pairwise relationships between all positions. This ability to directly model long-range interactions without the vanishing gradient issues of recurrence has made it highly influential across machine learning domains and, more recently, hydrology (Castangia et al., 2023; Demiray et al., 2024; Koya and Roy, 2024).

At its core, the Transformer architecture begins by mapping input sequences into a continuous embedding space. Each input vector is first passed through a linear embedding layer that projects raw features into a shared hidden dimension. Since the architecture does not inherently encode temporal order, positional encodings are then added to these embeddings to provide information about sequence structure. This ensures that the model can distinguish between inputs at different time steps.

The encoded sequence is subsequently processed by a stack of Transformer encoder layers, each containing two primary submodules: multi-head self-attention and position-wise feed-forward networks. In the self-attention step, each embedded vector is linearly projected into query, key, and value representations. Pairwise similarity between queries and keys defines attention weights, which are applied to the values to compute context-aware representations. Multi-head attention extends this process by allowing the model to capture dependencies at multiple temporal scales in parallel. The resulting representations are passed through feed-forward networks applied independently to each position, enabling nonlinear transformations. Residual connections and layer normalization are applied around each sublayer to stabilize optimization and improve gradient flow.

By combining embeddings, positional encodings, and stacked attention—feed-forward blocks, the Transformer can flexibly capture both short- and long-range dependencies in sequential data. Unlike recurrent architecture, which process inputs sequentially, Transformer architecture leverages parallel computation across time steps, offering significant efficiency gains while modeling complex temporal patterns.

In this study, the Transformer benchmark employs a compact encoder-only design with a single encoder block, eight attention heads, a hidden dimension of 256, and a model dimension of 64, combined with a dropout rate of 0.4 to mitigate overfitting. Input sequences are first projected through a linear embedding layer, after which learnable positional embeddings are added to encode temporal order. For the single-task Transformer, this embedding scheme provides the sole representation of position and input features. In the multi-task variant, an additional task embedding is introduced: following positional encoding, a learned task vector is added to the sequence embeddings, where task identifiers distinguish between streamflow (task ID = 0) and soil moisture (task ID = 1). This design enables the model to differentiate tasks within a shared architecture without introducing task-specific encoders or decoders. After the

encoder block, a fully connected output layer maps the representation to the final prediction. Together, these design choices yield a streamlined yet flexible framework for evaluating embedding-based task conditioning in hydrological forecasting.

The adoption of Transformers in hydrology is growing, with studies reporting improved predictive skill relative to RNNs and better interpretability through attention weights (Amanambu et al., 2022; Xu et al., 2023; Li et al., 2024; Demiray et al., 2025). By incorporating Transformers in our comparison, we aim to test whether their flexible handling of long-range dependencies can complement an embedding-based multi-task setup. This provides a direct benchmark against recurrent models, clarifying whether attention-driven representations offer tangible advantages when a model must distinguish between multiple hydrological tasks.

2.2.3. Mamba Model

The Mamba architecture represents a recent development in sequence modeling, designed to combine the efficiency of state-space models with the representational flexibility of deep learning (Gu & Dao, 2023). Unlike recurrent networks, which propagate information step by step, or Transformers, which explicitly compute pairwise interactions across sequences, Mamba leverages a structured state-space representation to model long sequences through fast parallelizable updates. This formulation enables it to capture both local dependencies and long-range memory while maintaining favorable computational complexity, scaling linearly with sequence length rather than quadratically as in self-attention. These properties have made Mamba an emerging alternative to Transformers for domains where long sequences and efficiency are critical.

At its core, Mamba processes sequences through a selective state-space mechanism. Each input is projected into a latent state, which is iteratively updated using parameterized dynamics that balance stability and adaptability. A selective scan operation governs how past states contribute to current representations, enabling the model to retain relevant long-term information while discarding redundancy. The outputs are then transformed through projection layers to produce the final sequence representation. By integrating these components into a deep stack with residual connections and normalization, Mamba can model complex temporal dynamics without the bottlenecks of recurrence or the computational burden of dense attention.

For hydrological forecasting, where long input windows and high-dimensional forcings are common, such efficiency and scalability are appealing. Although Mamba is not yet widely adopted in the field, its ability to process extended sequences with reduced resource requirements suggests strong potential for data-rich and computationally demanding applications. Recent studies have begun to explore its utility for hydrological prediction, highlighting both its promise and its novelty (Jia et al., 2024; Demiray and Demir, 2025).

In this study, we implemented both single-task and multi-task variants of Mamba. The baseline configuration employed a compact encoder-style design with a model dimension of 128 to represent the latent space of the input sequence, a state dimension of 4 to control the size of the hidden state in the selective state-space update, a convolutional kernel size of 2 to capture

local temporal interactions, and an expansion factor of 2 to increase the capacity of the intermediate feed-forward representations. A dropout rate of 0.4 was applied for regularization. As with the Transformer, the input features were first mapped into a latent space using a linear embedding layer, and positional encodings were then incorporated to preserve information about temporal order within the sequence. In the single-task Mamba, these embeddings formed the complete input representation.

For the multi-task version, we introduced an additional trainable task embedding after positional encoding, a task vector was added to the input sequence, with task identifiers distinguishing between streamflow (task ID = 0) and soil moisture (task ID = 1). This modification enabled the model to differentiate tasks within a shared architecture without introducing separate model branches. After processing through the Mamba layer, a final linear layer produced the model outputs. By incorporating Mamba into our comparison, we evaluate whether embedding-based multi-task learning benefits from state-space dynamics in addition to recurrent and attention-based designs. While still novel in hydrology, Mamba's efficiency and ability to capture dependencies across long input windows make it a promising candidate for future large-scale forecasting applications.

2.3. Training Setup

All models were trained under a consistent experimental setup using PyTorch to ensure comparability. The input consisted of 41 dynamic (time-series) variables and 211 static catchment attributes, concatenated to form a feature space of 252 dimensions. For single-task models, the input tensor was structured as [samples, 365, 252], where 365 represents the past year of daily observations used to predict future conditions. No future information was included in the inputs. For the multi-task models, the same input features used in the single-task setting were provided together with a task identifier (0 for streamflow and 1 for soil moisture), expressed as (historical data, task id). This identifier was passed through a task embedding layer and added to the input representation, allowing the model to distinguish between tasks while sharing a common architecture. The model outputs were defined as a 7-day forecast window, yielding tensors of shape [samples, 7].

Training employed the Adam optimizer (Kingma and Ba, 2014) with a learning rate of 1×10^{-4} , and the loss function was set to mean squared error (MSE). For the multi-task experiments, the overall loss was defined as the mean of the task-specific MSE values for streamflow and soil moisture, ensuring balanced optimization across tasks. The models were trained with a batch size of 512 for a maximum of 100 epochs. To prevent overfitting, early stopping was applied with a patience of 16 epochs based on validation loss. Additionally, the learning rate was dynamically adjusted using a ReduceLROnPlateau scheduler with patience set to 5 epochs, reducing the rate when validation performance plateaued.

This setup ensured that all models—from recurrent baselines (LSTM, GRU) to attention- and state-space—based architectures (Transformer, Mamba)—were trained and evaluated under identical conditions. By holding hyperparameters and training procedures constant within the

PyTorch framework, differences in predictive skill can be attributed directly to architectural choices rather than optimization discrepancies.

2.4. Performance Metrics

Model performance was assessed using 11 complementary metrics that capture different aspects of predictive skill. Error-based measures included the Mean Squared Error (MSE), Root Mean Squared Error (RMSE), and Mean Absolute Error (MAE), which quantify the magnitude of deviations between predictions and observations. Relative error was evaluated using the Normalized RMSE (NRMSE) and the Mean Absolute Scaled Error (MASE), providing scale-independent assessments that facilitate comparison across basins of varying flow regimes.

To evaluate predictive efficiency and correlation, we employed the Nash–Sutcliffe Efficiency (NSE) and the Kling–Gupta Efficiency (KGE), two of the most widely used performance measures in hydrology. Correlation-based skill was assessed using both Pearson's correlation coefficient (r) and Spearman's rank correlation coefficient (ρ), allowing evaluation of linear as well as monotonic relationships between predicted and observed values.

Finally, two metrics were used to assess broader aspects of model agreement with observations: the Willmott Index of Agreement (d1), which measures relative error against the observed mean, and the Taylor Skill Score (TSS), which integrates correlation, variance, and error into a single diagnostic measure.

Each metric was computed separately for the 7-day prediction horizon, yielding daily scores across lead times. Results are presented as tables with seven rows (days) and model comparisons as columns. Given the large number of evaluations across two tasks (streamflow and soil moisture) and 11 metrics, we focus in the main text on a subset of representative metrics, while the full set of results is provided in the Appendix.

3. Results

This section presents the experimental evaluation of the proposed multi-task learning framework against established single-task baselines. The study focuses on two fundamental hydrological prediction tasks: streamflow forecasting and soil moisture forecasting, each formulated as a 7-day ahead prediction problem using the preceding 365 days of forcings and catchment attributes as input. To provide a comprehensive assessment, we employed 11 performance metrics spanning error magnitude, efficiency, correlation, and agreement. In the main text, we highlight four representative metrics—NSE, KGE, MSE, and the Willmott Index of Agreement (d1)—which collectively capture predictive accuracy and reliability. Results for the remaining seven metrics, which show similar trends, are reported in the Appendix.

The results are presented in two parts. The first section reports benchmark results across all models, focusing on the comparison between recurrent (LSTM, GRU), attention-based (Transformer), and state-space (Mamba) architectures in both their single-task and multi-task configurations. The second section introduces the explainability analysis, where SHAP values are used to interpret the learned relationships and identify key drivers of prediction skill. The

overarching goal of these experiments is not only to benchmark raw predictive skills, but also to demonstrate that the embedding-based multi-task models can effectively distinguish between hydrological tasks while maintaining accuracy comparable to single-task counterparts, as we emphasized earlier.

3.1. Benchmark Results

The benchmark evaluation covers both streamflow and soil moisture prediction tasks, each formulated as a 7-day forecast. Results are presented in Tables 1–8. Tables 1 and 2 summarize NSE values, Tables 3 and 4 report KGE, Tables 5 and 6 present MSE, and Tables 7 and 8 provide the Willmott Index of Agreement (d1). The remaining seven metrics are provided in the Appendix and demonstrate consistent trends. Together, these results allow us to evaluate the relative strengths of recurrent, attention-based, and state-space architectures, and to assess whether the proposed multi-task design performs comparably to specialized single-task counterparts.

Table 1: NSE results for the streamflow prediction task over the 7-day forecast horizon.

Day	GRU	LSTM	MambaDouble	Mamba	TransformerDouble	Transformer
1	0.735554	0.741544	0.768077	0.766200	0.751702	0.754617
2	0.565607	0.565005	0.577403	0.574322	0.567272	0.571014
3	0.492114	0.489381	0.499727	0.496541	0.492627	0.494794
4	0.452349	0.448757	0.456891	0.454804	0.453051	0.455383
5	0.425674	0.421506	0.429677	0.427092	0.426484	0.428776
6	0.408595	0.404856	0.410095	0.408805	0.410450	0.412202
7	0.396861	0.39408	0.397935	0.397355	0.397898	0.400194

Table 2. NSE results for the soil moisture prediction task over the 7-day forecast horizon.

Day	GRU	LSTM	MambaDouble	Mamba	TransformerDouble	Transformer
1	0.996095	0.996344	0.995136	0.996447	0.995082	0.995943
2	0.987530	0.987842	0.986393	0.98815	0.986337	0.987719
3	0.979380	0.979718	0.978085	0.980074	0.978008	0.979818
4	0.972295	0.972695	0.971063	0.973102	0.970707	0.972930
5	0.966170	0.966582	0.964695	0.967048	0.964208	0.966859
6	0.960791	0.961284	0.959187	0.961717	0.958431	0.96148
7	0.956095	0.956643	0.954191	0.956946	0.953283	0.956632

As shown in Table 1 (streamflow) and Table 2 (soil moisture), predictive efficiency declines with lead time as expected, with day-1 forecasts consistently outperforming day-7 forecasts. For streamflow, all architectures follow a similar downward trend, where Transformer and Mamba models tend to maintain marginally higher NSE toward day 7, although the differences remain small. Multi-task variants closely follow the trajectories of their single-task counterparts, with negligible differences across lead times; in some cases, the MambaDouble model even produces slightly higher NSE scores. Soil moisture prediction yields higher NSE values overall and exhibits less separation between architectures, reflecting the smoother dynamics of soil moisture compared to the rapid variability of streamflow.

Table 3. KGE results for the streamflow prediction task over the 7-day forecast horizon.

Day	GRU	LSTM	MambaDouble	Mamba	TransformerDouble	Transformer
1	0.774388	0.793430	0.816638	0.802474	0.778430	0.802229
2	0.633924	0.640799	0.649402	0.634635	0.636651	0.654970
3	0.563219	0.572056	0.582931	0.564508	0.568982	0.591008
4	0.529540	0.535417	0.538940	0.532156	0.531168	0.544917
5	0.504408	0.506991	0.507592	0.507273	0.504517	0.513616
6	0.485226	0.491321	0.499158	0.479134	0.486910	0.496711
7	0.471015	0.488316	0.478313	0.460941	0.474076	0.481934

Table 4. KGE results for the soil moisture prediction task over the 7-day forecast horizon.

Day	GRU	LSTM	MambaDouble	Mamba	TransformerDouble	Transformer
1	0.985944	0.997711	0.991607	0.995983	0.986162	0.986195
2	0.981290	0.993121	0.984901	0.993753	0.982488	0.981524
3	0.977953	0.987504	0.977293	0.989345	0.976971	0.975989
4	0.972852	0.982715	0.976657	0.980781	0.969591	0.970956
5	0.970103	0.978349	0.972026	0.976219	0.962193	0.966542
6	0.965747	0.975592	0.971567	0.971248	0.955717	0.962692
7	0.962278	0.973143	0.963859	0.969748	0.951808	0.959094

Results in Table 3 (streamflow) and Table 4 (soil moisture) show KGE trends consistent with the NSE findings: values decrease gradually across the 7-day horizon, with higher skill at short lead times. For streamflow, all six models perform closely, with differences rarely exceeding a few hundredths. Transformer and Mamba variants show slightly higher KGE at some horizons, while LSTM occasionally matches or exceeds them, particularly toward longer leads. Soil

moisture forecasts yield substantially higher absolute KGE values than streamflow, remaining above 0.95 even at day-7 for all models. Here, the separation between architectures is again minimal: LSTM and Mamba variants often lead, but Transformer and GRU remain highly competitive. The overall consistency across models reflects the smoother and more predictable dynamics of soil moisture compared to the variability of streamflow. Multi-task versions remain closely aligned with their single-task counterparts on both tasks, demonstrating that task embeddings preserve predictive skill without loss of stability.

Table 5. MSE results for the streamflow prediction task over the 7-day forecast horizon.

Day	GRU	LSTM	MambaDouble	Mamba	TransformerDouble	Transformer
1	3.695899	3.612172	3.241358	3.267590	3.470205	3.429462
2	6.070147	6.078551	5.905302	5.948367	6.046870	5.994587
3	7.081848	7.119968	6.975696	7.020126	7.074707	7.044486
4	7.599153	7.648990	7.536130	7.565085	7.589408	7.557058
5	7.965754	8.023550	7.910222	7.946081	7.954518	7.922718
6	8.201715	8.253564	8.180912	8.198794	8.175986	8.151683
7	8.360973	8.399528	8.346082	8.35413	8.346593	8.314768

Table 6. MSE results for the soil moisture prediction task over the 7-day forecast horizon.

Day	GRU	LSTM	MambaDouble	Mamba	TransformerDouble	Transformer
1	0.000460	0.000430	0.000573	0.000418	0.000579	0.000478
2	0.001468	0.001432	0.001602	0.001395	0.001609	0.001446
3	0.002428	0.002388	0.002581	0.002346	0.002590	0.002377
4	0.003263	0.003215	0.003408	0.003167	0.003450	0.003188
5	0.003984	0.003935	0.004158	0.003881	0.004215	0.003903
6	0.004617	0.004559	0.004806	0.004508	0.004895	0.004536
7	0.005170	0.005106	0.005395	0.005070	0.005502	0.005107

As shown in Table 5 (streamflow) and Table 6 (soil moisture), mean squared errors increase predictably with lead time. For streamflow, values rise from around 3–4 on day 1 to about 8 by day 7, yet the progression is nearly parallel across all six models. Small variations are visible—for example, MambaDouble and Transformer often yield slightly lower errors, while GRU tends to be marginally higher—but these differences are minor relative to the overall magnitude of error. Multi-task models reproduce the error patterns of their single-task counterparts with no noticeable divergence. For soil moisture, MSE values are several orders of magnitude smaller

(<0.006 at day 7), and the curves across models are almost indistinguishable. Occasional small advantages for LSTM or Mamba are within the same decimal precision as the other models. The consistently low errors highlight the smoother dynamics of soil moisture and confirm that the multi-task framework preserves accuracy on par with single-task approaches.

Table 7. Willmott Index of Agreement (d1) results for the streamflow prediction task over the 7-day forecast horizon.

Day	GRU	LSTM	MambaDouble	Mamba	TransformerDouble	Transformer
1	0.851651	0.857549	0.864039	0.865897	0.859252	0.859084
2	0.795670	0.801725	0.804046	0.803968	0.802629	0.802625
3	0.762577	0.765187	0.771712	0.764553	0.767840	0.770160
4	0.741043	0.743132	0.748861	0.744854	0.746569	0.752623
5	0.727078	0.729312	0.731526	0.728401	0.732207	0.739353
6	0.713301	0.719571	0.719289	0.716756	0.721658	0.729445
7	0.704124	0.712325	0.710625	0.713556	0.712638	0.720848

Table 8. Willmott Index of Agreement (d1) results for the soil moisture prediction task over the 7-day forecast horizon.

Day	GRU	LSTM	MambaDouble	Mamba	TransformerDouble	Transformer
1	0.974125	0.975426	0.970985	0.975534	0.970782	0.973207
2	0.953874	0.955309	0.950436	0.955825	0.951047	0.954252
3	0.937767	0.939477	0.934257	0.940081	0.935048	0.938532
4	0.925612	0.927727	0.923892	0.927570	0.922741	0.926773
5	0.916615	0.918700	0.914426	0.918832	0.912940	0.917645
6	0.909224	0.911779	0.907677	0.911516	0.905019	0.910329
7	0.903280	0.906134	0.900810	0.905379	0.898685	0.904217

Agreement values in Table 7 (streamflow) and Table 8 (soil moisture) remain consistently high, reflecting strong alignment between predictions and observations across all models. For streamflow, d1 values start around 0.85 on day-1 and decline gradually to just above 0.70 by day-7. Differences between models are small, typically within a few hundredths, with Transformer and Mamba variants sometimes slightly ahead but not by a margin large enough to indicate systematic advantage. The multi-task versions closely reproduce the patterns of their single-task counterparts, confirming that task embeddings do not diminish agreement. Soil moisture forecasts yield even higher agreement values, above 0.97 at day-1 and remaining near

0.90 at day-7. Here too, the separation between models is negligible: all six architectures track nearly identical trajectories. The uniformly high values highlight the relative stability of soil moisture predictions and further illustrate that the multi-task framework maintains reliability on par with single-task baselines.

Across all metrics, three consistent findings emerge. First, forecast skill declines with lead time for every model, with the effect more pronounced for streamflow than for soil moisture. This reduction is expected because our setup relies solely on past observations as input; no predictive information from future meteorological forcings is included. While some studies incorporate forecasted forcings to mitigate performance loss at longer horizons, our models do not, which explains why day-1 predictions are consistently strong, but skill diminishes over the week. Streamflow, being more sensitive to short-term variability and extremes, shows a sharper reduction in efficiency beyond the first few days, whereas soil moisture forecasts remain comparatively stable across the 7-day horizon.

Second, across the horizon, the differences among architectures are generally modest. Transformer and Mamba tend to achieve slightly higher scores in several cases, while LSTM and GRU remain competitive and in some instances outperform on certain metrics, particularly for soil moisture. Third, and most importantly, the multi-task models perform comparably to their single-task counterparts across all experiments. Even without task-specific encoders or decoders, the use of task embeddings enables the shared model to correctly distinguish objectives and deliver predictions of similar quality. In some cases, the double-task variants even slightly outperform the single-task baselines, reinforcing the feasibility of embedding-based task conditioning for hydrological forecasting.

Finally, results for the remaining seven metrics—MAE, RMSE, NRMSE, Pearson's r, Spearman's ρ , MASE, and the Taylor Skill Score—are presented in the Appendix and confirm the same overall patterns. These complementary evaluations strengthen confidence in the robustness of the findings and demonstrate that the observed trends are not confined to a small subset of performance measures.

3.2. Explainability Analysis

To complement the benchmark comparisons, we conducted an explainability analysis using SHapley Additive exPlanations (SHAP). SHAP is a unified framework for feature attribution that draws from cooperative game theory (Lundberg and Lee, 2017). Each model prediction is represented as the sum of contributions from individual input features, where the contribution of a feature is computed as its average marginal effect across all possible subsets of inputs. This property ensures both local accuracy (the attributions sum to the model output) and consistency (if a feature has a greater effect in one model than another, its importance cannot decrease). These advantages make SHAP one of the most widely used tools for interpreting modern machine learning models. In hydrology, explainability is crucial not only for model transparency but also for verifying whether learned drivers are consistent with physical understanding. SHAP

provides a direct way to examine whether multi-task learning preserves task-specific feature relevance when tasks share the same input space.

For this study, SHAP values were computed with 10,000 training samples as background data, establishing the feature distribution against which marginal contributions were evaluated. For the test phase, 1,000 samples per task (streamflow and soil moisture) were used to generate SHAP explanations. To summarize feature importance, we calculated the mean absolute SHAP value (mean|SHAP|) for each predictor and then extracted the top 15 features per model and per task. For the multi-task models, we also concatenated the SHAP values for both tasks (2,000 samples total) and reported the top 20 features from this combined perspective. These rankings are shown in Figures 2–4.

Figure 2 presents the top 15 features for the streamflow task across all models. Lagged streamflow emerges as the most influential predictor, reflecting the strong autoregressive memory inherent in discharge series. Beyond this dominant signal, soil water content layers consistently rank highly, highlighting the role of catchment storage and infiltration in shaping runoff response. Temperature variables, particularly daily minima and maxima, also appear as important drivers, consistent with their influence on snowmelt and evapotranspiration processes.

Architectural differences are visible in how meteorological variables are weighed. Transformer models assign greater importance to surface pressure features, suggesting that the attention mechanism captures atmospheric state information more directly. In contrast, MambaDouble elevates precipitation-related inputs, while the single-task Mamba relies more heavily on soil water and temperature. Despite these differences, the overall set of influential features remains consistent across models. Importantly, the multi-task variants reproduce the similar dominant drivers as the single-task counterparts, showing that the inclusion of multiple tasks does not dilute the identification of streamflow-relevant predictors.

Figure 3 presents the top 15 features for the soil moisture task across all models. Unlike streamflow, where a single autoregressive feature dominates, soil moisture predictions are shaped primarily by depth-resolved soil water content variables. Maxima, minima, and means from the first three layers consistently rank highest, reflecting both their abundance in the dataset and their direct physical relevance. Since the dataset provides multiple descriptors of soil water conditions across depths (0–7 cm, 7–28 cm, 28–100 cm, 100–289 cm) in addition to the aggregated soil moisture index, these variables naturally dominate the importance rankings. Their prevalence highlights the strong vertical coupling of soil water dynamics, where the state of one layer constrains retention, recharge, and drainage in others.

Secondary contributions come from atmospheric variables, particularly surface pressure, evaporation, and radiation indices, which modulate infiltration and drying processes. Architectural differences are again evident: Transformer models assign relatively greater weight to pressure variables, while Mamba models emphasize the soil water features themselves.

An important observation is that the constructed target feature—the mean soil moisture index derived from all four layers—does not appear among the top drivers. Instead, the models rely more heavily on minima and maxima from individual layers, which capture dynamic soil

conditions such as saturation or drought more effectively than aggregated means. This indicates that the models are not simply reproducing the target from itself but are leveraging related depth-specific descriptors that provide complementary information.

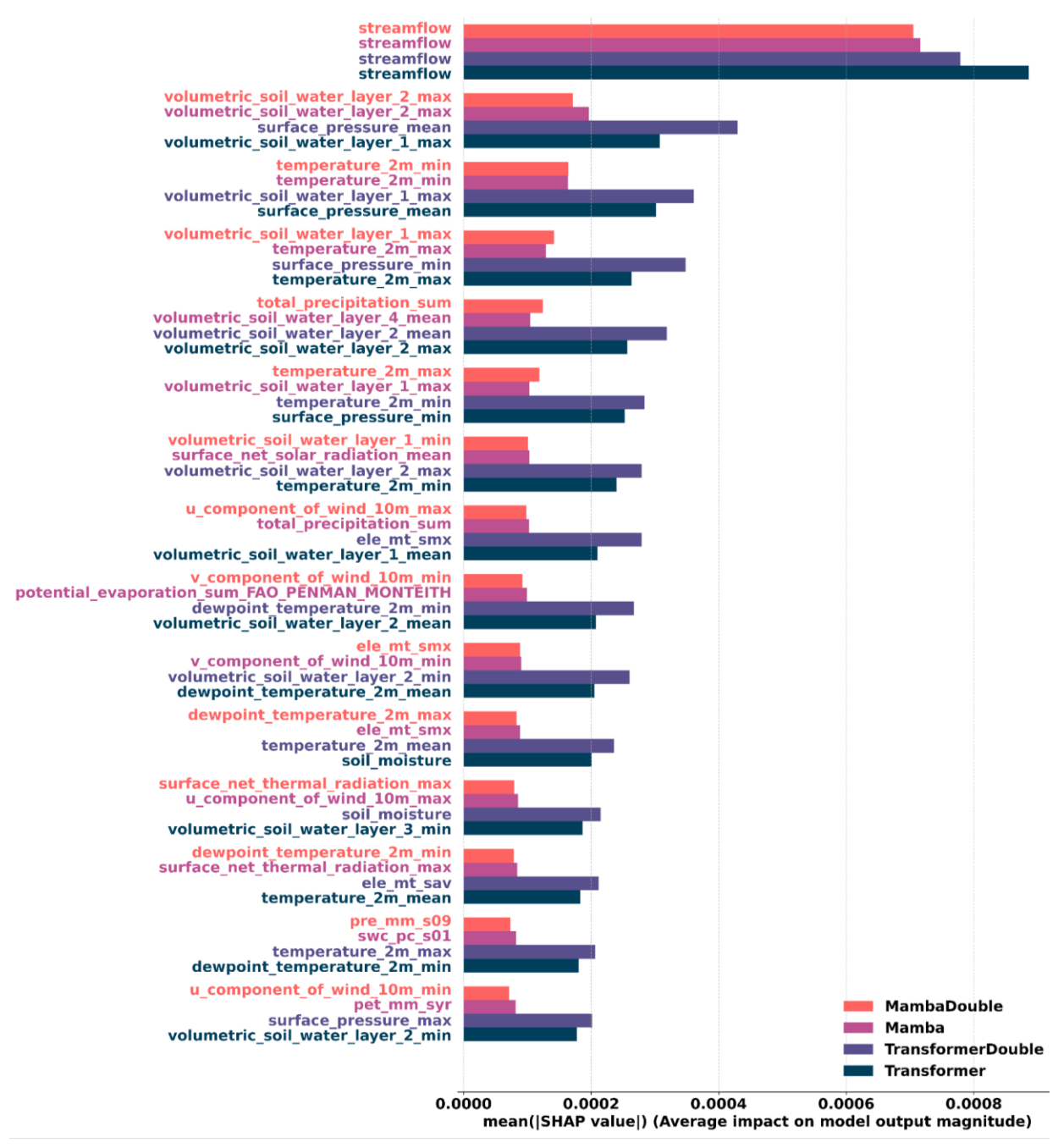


Figure 2: Top 15 features for the streamflow task across all models

Across both single-task and multi-task models, the centrality of these layered soil water features is consistent, with atmospheric variables such as pressure and evaporation providing secondary modulation. Together, these patterns highlight that soil moisture prediction is governed less by a single aggregated metric and more by the interplay of depth-resolved extremes and atmospheric forcing, reflecting both the structure of the dataset and underlying hydrological processes.

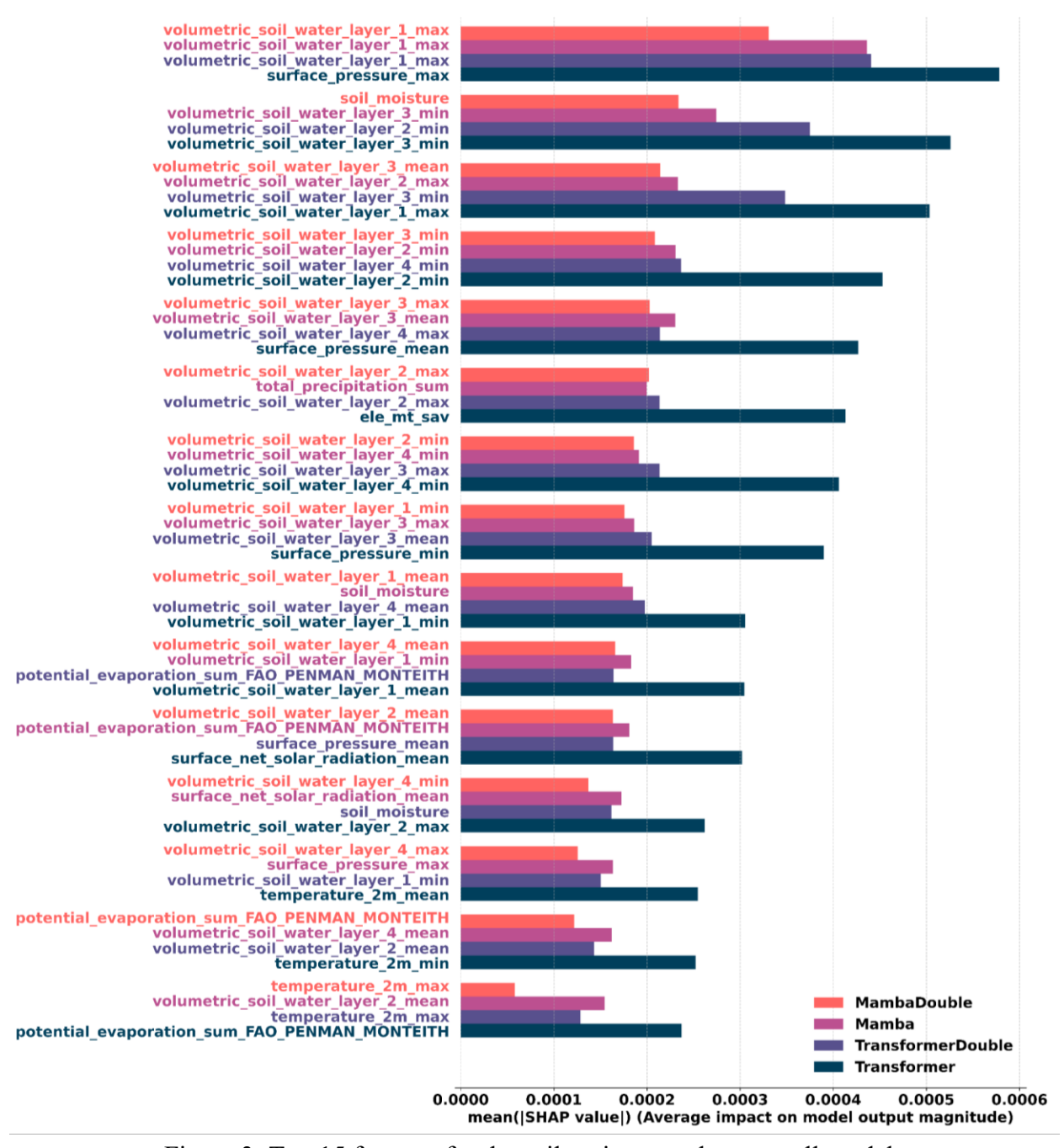


Figure 3: Top 15 features for the soil moisture task across all models

Finally, Figure 4 presents the top 20 features from the combined-task analysis for the multitask models, where SHAP values for streamflow and soil moisture were evaluated jointly. Based on the analysis, lagged streamflow remains the single most important driver overall, consistent with the strong autoregressive control of discharge dynamics. At the same time, soil water content variables across depths account for the majority of the top-ranked features, reflecting their central role in predicting soil moisture and their contribution to runoff generation.

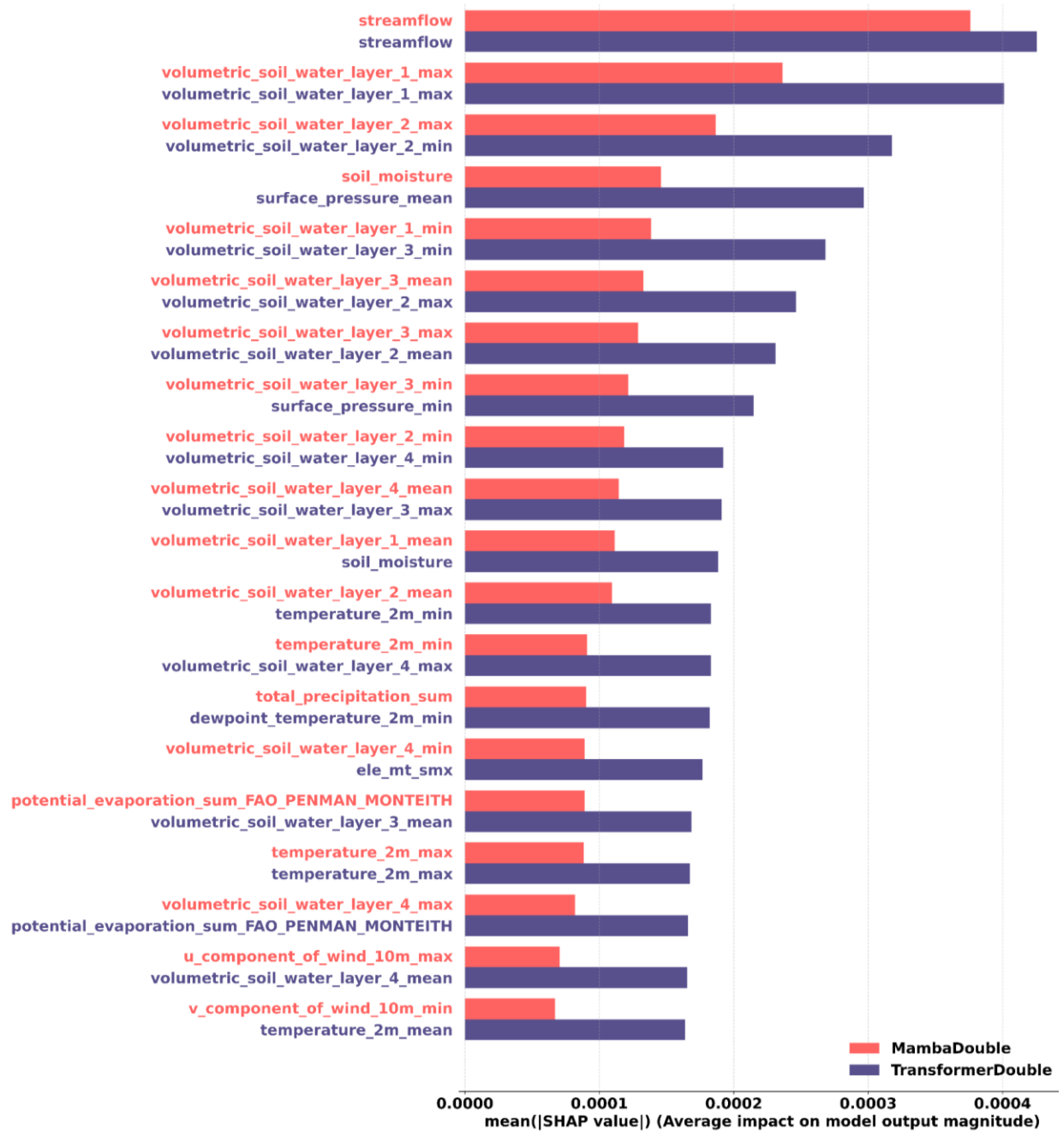


Figure 4: Top 20 combined-task features for MambaDouble and TransformerDouble models

The presence of both categories at the top of the rankings illustrates that the model successfully distinguishes between task-specific drivers even within a shared architecture. Streamflow-related predictors—lagged discharge, precipitation, and temperature—remain

prominent without overshadowing the soil variables, while depth-resolved soil moisture features retain their influence without diluting the importance of discharge history. Secondary atmospheric predictors, such as surface pressure and radiation, appear in mid-ranks, reflecting their relevance to both tasks through controls on infiltration, evaporation, and catchment energy balance.

Overall, the combined-task perspective demonstrates that the multi-task models capture a balanced mixture of streamflow and soil moisture drivers rather than converging on a single set of features. This balance reinforces the conclusion that introducing multiple tasks does not blur feature attribution: streamflow remains conditioned by its own history and climatic inputs, while soil moisture predictions are governed primarily by layered soil states and evaporative demand.

Taken together, the SHAP analyses demonstrate that the models learn task-specific drivers that are both physically meaningful and consistent across architectures. For streamflow, predictions are anchored by the autoregressive influence of past discharge, modulated by soil storage, temperature, and precipitation. For soil moisture, the dominant controls are depthresolved soil water content features, supplemented by atmospheric and energy-related variables, with the models favoring dynamic descriptors such as layer minima and maxima rather than aggregated averages.

The combined-task results further show that multi-task models preserve this separation of drivers: streamflow predictors remain centered on discharge history, while soil moisture predictions draw primarily on layered soil states, with no evidence of conflation between the two. These findings highlight that introducing multiple tasks does not dilute attribution patterns and confirm that the models remain sensitive to the hydrological processes most relevant for each target.

4. Conclusion

This study investigated multi-task learning for hydrological forecasting, focusing on daily streamflow and soil moisture prediction across 628 basins from the CAMELS-US dataset within CARAVAN. Recurrent (LSTM, GRU), attention-based (Transformer), and state-space (Mamba) architectures were evaluated in both single-task and multi-task settings over a 7-day forecast horizon using eleven performance metrics.

Our findings highlight three consistent themes. First, predictive skill declines with lead time as expected, particularly for streamflow, reflecting the absence of forecasted meteorological inputs and the high sensitivity of flow to short-term variability. Soil moisture forecasts, by contrast, remain comparatively stable across the week, benefiting from smoother temporal dynamics. Second, across all metrics, differences between architectures are modest. Transformer and Mamba models tend to achieve slightly higher scores in several cases, but LSTM and GRU remain competitive, underscoring the robustness of recurrent approaches. Third, and most importantly, the multi-task variants achieve performance comparable to their single-task counterparts. Even without task-specific encoders or decoders, the use of task embeddings

enabled the shared backbone to differentiate between tasks and produce reliable forecasts. This demonstrates that embedding-based task conditioning is feasible for hydrological applications.

Explainability analyses using SHAP further confirmed that the models remained task-aware and physically interpretable, with task identifiers enabling a shared architecture to separate the drivers of streamflow and soil moisture. Streamflow forecasts were governed primarily by lagged flow, soil water states, and meteorological forcings, while soil moisture forecasts were dominated by depth-resolved soil water content and supplemented by atmospheric and energy-related drivers. The multi-task variants preserved these attribution patterns, demonstrating that introducing multiple tasks did not blur the distinction between streamflow and soil moisture drivers.

While accuracy gains over single-task baselines were limited, the results establish a proof of concept: a single DL model can represent multiple hydrological tasks when guided only by a task identifier. This foundation opens the door to more ambitious directions, including the integration of additional targets such as evapotranspiration, water temperature, or rainfall downscaling, the use of forecasted forcings to extend skill at longer horizons, and the eventual development of general-purpose hydrological AI systems. By showing that multi-task learning is both practical and interpretable, this study marks a step toward more unified and efficient approaches to environmental prediction.

References

- Abbes, A.B., Jarray, N. and Farah, I.R., 2024. Advances in remote sensing based soil moisture retrieval: applications, techniques, scales and challenges for combining machine learning and physical models. Artificial Intelligence Review, 57(9), p.224.
- Addor, N., Newman, A.J., Mizukami, N. and Clark, M.P., 2017. The CAMELS data set: catchment attributes and meteorology for large-sample studies. Hydrology and Earth System Sciences, 21(10), pp.5293-5313.
- Alabbad, Y., Yildirim, E., & Demir, I. (2023). A web-based analytical urban flood damage and loss estimation framework. *Environmental Modelling & Software*, *163*, 105670.
- Alvarez-Garreton, C., Mendoza, P.A., Boisier, J.P., Addor, N., Galleguillos, M., Zambrano-Bigiarini, M., Lara, A., Puelma, C., Cortes, G., Garreaud, R. and McPhee, J., 2018. The CAMELS-CL dataset: catchment attributes and meteorology for large sample studies—Chile dataset. Hydrology and Earth System Sciences, 22(11), pp.5817-5846.
- Amanambu, A.C., Mossa, J. and Chen, Y.H., 2022. Hydrological drought forecasting using a deep transformer model. Water, 14(22), p.3611.
- Arsenault, R., Brissette, F., Martel, J.L., Troin, M., Lévesque, G., Davidson-Chaput, J., Gonzalez, M.C., Ameli, A. and Poulin, A., 2020. A comprehensive, multisource database for hydrometeorological modeling of 14,425 North American watersheds. Scientific Data, 7(1), p.243.

- Arsenault, R., Martel, J.L., Brunet, F., Brissette, F. and Mai, J., 2023. Continuous streamflow prediction in ungauged basins: long short-term memory neural networks clearly outperform traditional hydrological models. Hydrology and Earth System Sciences, 27(1), pp.139-157.
- Barrault, L., Chung, Y.A., Meglioli, M.C., Dale, D., Dong, N., Duquenne, P.A., Elsahar, H., Gong, H., Heffernan, K., Hoffman, J. and Klaiber, C., 2023. SeamlessM4T: massively multilingual & multimodal machine translation. arXiv preprint arXiv:2308.11596.
- Bommasani, R., 2021. On the opportunities and risks of foundation models. arXiv preprint arXiv:2108.07258.
- Brown, T., Mann, B., Ryder, N., Subbiah, M., Kaplan, J.D., Dhariwal, P., Neelakantan, A., Shyam, P., Sastry, G., Askell, A. and Agarwal, S., 2020. Language models are few-shot learners. Advances in neural information processing systems, 33, pp.1877-1901.
- Caruana, R., 1997. Multitask learning. Machine learning, 28(1), pp.41-75.
- Castangia, M., Grajales, L. M. M., Aliberti, A., Rossi, C., Macii, A., Macii, E., & Patti, E. (2023). Transformer neural networks for interpretable flood forecasting. Environmental Modelling & Software, 160, 105581.
- Cho, K., Van Merriënboer, B., Gulcehre, C., Bahdanau, D., Bougares, F., Schwenk, H. and Bengio, Y., 2014. Learning phrase representations using RNN encoder-decoder for statistical machine translation. arXiv preprint arXiv:1406.1078.
- Chung, J., Gulcehre, C., Cho, K. and Bengio, Y., 2014. Empirical evaluation of gated recurrent neural networks on sequence modeling. arXiv preprint arXiv:1412.3555.
- Cikmaz, B. A., Yildirim, E., & Demir, I. (2025). Flood susceptibility mapping using fuzzy analytical hierarchy process for Cedar Rapids, Iowa. *International journal of river basin management*, 23(1), 1-13.
- Coxon, G., Addor, N., Bloomfield, J.P., Freer, J., Fry, M., Hannaford, J., Howden, N.J., Lane, R., Lewis, M., Robinson, E.L. and Wagener, T., 2020. CAMELS-GB: hydrometeorological time series and landscape attributes for 671 catchments in Great Britain. Earth System Science Data Discussions, 2020, pp.1-34.
- Davenport, F.V., Burke, M. and Diffenbaugh, N.S., 2021. Contribution of historical precipitation change to US flood damages. Proceedings of the National Academy of Sciences, 118(4), p.e2017524118.
- Demir, I., Conover, H., Krajewski, W.F., Seo, B.C., Goska, R., He, Y., McEniry, M.F., Graves, S.J. and Petersen, W., (2015). Data-enabled field experiment planning, management, and research using cyberinfrastructure. *Journal of Hydrometeorology*, *16*(3), pp.1155-1170.
- Demir, I., Xiang, Z., Demiray, B., & Sit, M. (2022). Waterbench: a large-scale benchmark dataset for data-driven streamflow forecasting. *Earth System Science Data Discussions*, 2022, 1-19.
- Demiray, B.Z., Sit, M., Mermer, O. and Demir, I., 2024. Enhancing hydrological modeling with transformers: a case study for 24-h streamflow prediction. Water Science & Technology, 89(9), pp.2326-2341.

- Demiray, B.Z. and Demir, I., 2024. Towards Generalized Hydrological Forecasting using Transformer Models for 120-Hour Streamflow Prediction. arXiv preprint arXiv:2406.07484.
- Demiray, B.Z. and Demir, I., 2025. Advancing Long-Horizon Hydrological Forecasting: A Mamba-based Approach with Explainable AI for Generalized Streamflow Prediction. EarthArxiv, 10109. https://doi.org/10.31223/X5B164
- Demiray, B.Z., Mermer, O., Baydaroğlu, Ö. and Demir, I., 2025. Predicting harmful algal blooms using explainable deep learning models: A comparative study. Water, 17(5), p.676.
- Devlin, J., Chang, M.W., Lee, K. and Toutanova, K., 2019, June. Bert: Pre-training of deep bidirectional transformers for language understanding. In Proceedings of the 2019 conference of the North American chapter of the association for computational linguistics: human language technologies, volume 1 (long and short papers) (pp. 4171-4186).
- ElSaadani, M., Habib, E., Abdelhameed, A.M. and Bayoumi, M., 2021. Assessment of a spatiotemporal deep learning approach for soil moisture prediction and filling the gaps in between soil moisture observations. Frontiers in artificial intelligence, 4, p.636234.
- Fang, J., Yang, L., Wen, X., Yu, H., Li, W., Adamowski, J.F. and Barzegar, R., 2024. Ensemble learning using multivariate variational mode decomposition based on the Transformer for multi-step-ahead streamflow forecasting. Journal of Hydrology, 636, p.131275.
- Fowler, K.J., Acharya, S.C., Addor, N., Chou, C. and Peel, M.C., 2021. CAMELS-AUS: hydrometeorological time series and landscape attributes for 222 catchments in Australia. Earth System Science Data Discussions, 2021, pp.1-30.
- Gao, L., Gao, Q., Zhang, H., Li, X., Chaubell, M.J., Ebtehaj, A., Shen, L. and Wigneron, J.P., 2022. A deep neural network based SMAP soil moisture product. Remote Sensing of Environment, 277, p.113059.
- Gu, A. and Dao, T., 2023. Mamba: Linear-time sequence modeling with selective state spaces. arXiv preprint arXiv:2312.00752.
- Hochreiter, S. and Schmidhuber, J., 1997. Long short-term memory. Neural computation, 9(8), pp.1735-1780.
- Hu, Y., Jiang, Y., Yao, H., Chen, Y., Wu, X., & Li, X. (2024). Effects of stacking LSTM with different patterns and input schemes on streamflow and water quality simulation. Available at SSRN 4620903.
- Huang, F., Yi, P., Chen, J. and Yang, J., 2023, May. A multi-Task Water Level Prediction Method Based on Attention Mechanism and LSTM. In 2023 6th International Conference on Artificial Intelligence and Big Data (ICAIBD) (pp. 639-643). IEEE.
- IPCC. (2021). Climate Change 2021: The Physical Science Basis. Contribution of Working Group I to the Sixth Assessment Report of the Intergovernmental Panel on Climate Change. Cambridge University Press.
- IPCC. (2023). In: Climate Change 2023: Synthesis Report. Contribution of Working Groups I, II and III to the Sixth Assessment Report of the Intergovernmental Panel on Climate Change [Core Writing Team, H. Lee and J. Romero (eds.)]. IPCC, Geneva, Switzerland, pp. 35-115, doi: 10.59327/IPCC/AR6-9789291691647.

- Islam, S. S., Yeşilköy, S., Baydaroğlu, Ö., Yıldırım, E., & Demir, I. (2025). State-level multidimensional agricultural drought susceptibility and risk assessment for agriculturally prominent areas. *International Journal of River Basin Management*, 23(2), 337-354.
- Jia, D., Li, W., Huang, D. and Chen, S., 2024. Daily runoff prediction based on lightweight Mamba with partial normalization. Hydrology Research, 55(12), pp.1182-1196.
- Khandelwal, A., Xu, S., Li, X., Jia, X., Stienbach, M., Duffy, C., ... & Kumar, V. (2020). Physics guided machine learning methods for hydrology. arXiv preprint arXiv:2012.02854.
- Kingma, D.P. and Ba, J., 2014. Adam: A method for stochastic optimization. arXiv preprint arXiv:1412.6980.
- Klingler, C., Schulz, K. and Herrnegger, M., 2021. Lamah large-sample data for hydrology and environmental sciences for central europe. Earth System Science Data Discussions, 2021, pp.1-46.
- Koya, S. R., & Roy, T. (2024). Temporal Fusion Transformers for streamflow Prediction: Value of combining attention with recurrence. Journal of Hydrology, 637, 131301.
- Kratzert, F., Klotz, D., Shalev, G., Klambauer, G., Hochreiter, S. and Nearing, G., 2019. Towards learning universal, regional, and local hydrological behaviors via machine learning applied to large-sample datasets. Hydrology and Earth System Sciences, 23(12), pp.5089-5110.
- Kratzert, F., Klotz, D., Hochreiter, S. and Nearing, G.S., 2021. A note on leveraging synergy in multiple meteorological datasets with deep learning for rainfall-runoff modeling. Hydrology and Earth System Sciences, 25, 2685–2703, https://doi.org/10.5194/hess-25-2685-2021.
- Kratzert, F., Nearing, G., Addor, N., Erickson, T., Gauch, M., Gilon, O., Gudmundsson, L., Hassidim, A., Klotz, D., Nevo, S. and Shalev, G., 2023. Caravan-A global community dataset for large-sample hydrology. Scientific Data, 10(1), p.61.
- Le, X.H., Nguyen, D.H., Jung, S., Yeon, M. and Lee, G., 2021. Comparison of deep learning techniques for river streamflow forecasting. IEEE Access, 9, pp.71805-71820.
- Lehner, B., Linke, S. & Thieme, M. 2019. HydroATLAS version 1.0. https://doi.org/10.6084/m9.figshare.9890531.v1
- Li, L., Dai, Y., Shangguan, W., Wei, Z., Wei, N. and Li, Q., 2022. Causality-structured deep learning for soil moisture predictions. Journal of Hydrometeorology, 23(8), pp.1315-1331.
- Li, B., Li, R., Sun, T., Gong, A., Tian, F., Khan, M. Y. A., & Ni, G. (2023). Improving LSTM hydrological modeling with spatiotemporal deep learning and multi-task learning: A case study of three mountainous areas on the Tibetan Plateau. Journal of Hydrology, 620, 129401.
- Li, X., Sun, Q.L., Zhang, Y., Sha, J. and Zhang, M., 2024. Enhancing hydrological extremes prediction accuracy: Integrating diverse loss functions in Transformer models. Environmental Modelling & Software, 177, p.106042.
- Linke, S., Lehner, B., Ouellet Dallaire, C., Ariwi, J., Grill, G., Anand, M., Beames, P., Burchard-Levine, V., Maxwell, S., Moidu, H. and Tan, F., 2019. Global hydro-environmental subbasin and river reach characteristics at high spatial resolution. Scientific data, 6(1), p.283.

- Liu, Y., Hou, G., Huang, F., Qin, H., Wang, B. and Yi, L., 2022a. Directed graph deep neural network for multi-step daily streamflow forecasting. Journal of Hydrology, 607, p.127515.
- Liu, J., Rahmani, F., Lawson, K. and Shen, C., 2022b. A multiscale deep learning model for soil moisture integrating satellite and in situ data. Geophysical Research Letters, 49(7), p.e2021GL096847.
- Liu, J., Bian, Y., Lawson, K. and Shen, C., 2024. Probing the limit of hydrologic predictability with the Transformer network. Journal of Hydrology, 637, p.131389.
- Lu, J., Clark, C., Zellers, R., Mottaghi, R. and Kembhavi, A., 2022. Unified-io: A unified model for vision, language, and multi-modal tasks. arXiv preprint arXiv:2206.08916.
- Lu, J., Xie, Z., Chen, J., Li, M., Xu, C. and Cao, H., 2023, October. GC-SALM: Multi-Task Runoff Prediction Using Spatial-Temporal Attention Graph Convolution Networks. In 2023 IEEE International Conference on Systems, Man, and Cybernetics (SMC) (pp. 3633-3638). IEEE.
- Lundberg, S.M. and Lee, S.I., 2017. A unified approach to interpreting model predictions. Advances in neural information processing systems, 30.
- Mishra, A.K. and Singh, V.P., 2010. A review of drought concepts. Journal of hydrology, 391(1-2), pp.202-216.
- Muñoz-Sabater, J., Dutra, E., Agustí-Panareda, A., Albergel, C., Arduini, G., Balsamo, G., Boussetta, S., Choulga, M., Harrigan, S., Hersbach, H. and Martens, B., 2021. ERA5-Land: A state-of-the-art global reanalysis dataset for land applications. Earth system science data, 13(9), pp.4349-4383.
- Ng, K.W., Huang, Y.F., Koo, C.H., Chong, K.L., El-Shafie, A. and Ahmed, A.N., 2023. A review of hybrid deep learning applications for streamflow forecasting. Journal of Hydrology, 625, p.130141.
- NOAA National Centers for Environmental Information (NCEI), 2022. US billion-dollar weather and climate disasters. https://www.ncei.noaa.gov/access/monitoring/billions/, DOI:10.25921/stkw-7w73.
- Ouyang, W., Gu, X., Ye, L., Liu, X., & Zhang, C. (2023). Exploring Variable Synergy in Multi-Task Deep Learning for Hydrological Modeling. Authorea Preprints.
- Rabiei, S., Babaeian, E. and Grunwald, S., 2025. Surface and Subsurface Soil Moisture Estimation Using Fusion of SMAP, NLDAS-2, and SOLUS100 Data with Deep Learning. Remote Sens. 17, 659. https://doi.org/10.3390/rs17040659.
- Ruder, S., 2017. An overview of multi-task learning in deep neural networks. arXiv preprint arXiv:1706.05098.
- Sadler, J.M., Appling, A.P., Read, J.S., Oliver, S.K., Jia, X., Zwart, J.A. and Kumar, V., 2022. Multi-task deep learning of daily streamflow and water temperature. Water Resources Research, 58(4), p.e2021WR030138.
- Senanayake, I.P., Pathira Arachchilage, K.R., Yeo, I.Y., Khaki, M., Han, S.C. and Dahlhaus, P.G., 2024. Spatial downscaling of satellite-based soil moisture products using machine learning techniques: A review. Remote Sensing, 16(12), p.2067.

- Seneviratne, S.I., Corti, T., Davin, E.L., Hirschi, M., Jaeger, E.B., Lehner, I., Orlowsky, B. and Teuling, A.J., 2010. Investigating soil moisture–climate interactions in a changing climate: A review. Earth-Science Reviews, 99(3-4), pp.125-161.
- Seo, B. C., Keem, M., Hammond, R., Demir, I., & Krajewski, W. F. (2019). A pilot infrastructure for searching rainfall metadata and generating rainfall product using the big data of NEXRAD. *Environmental modelling & software*, 117, 69-75.
- Sit, M., Demiray, B.Z., Xiang, Z., Ewing, G.J., Sermet, Y. and Demir, I., 2020. A comprehensive review of deep learning applications in hydrology and water resources. Water Science and Technology, 82(12), pp.2635-2670.
- Sit, M., Demiray, B. and Demir, I., 2021. Short-term hourly streamflow prediction with graph convolutional gru networks. arXiv preprint arXiv:2107.07039.
- Sit, M., Demiray, B.Z. and Demir, I., 2022. A systematic review of deep learning applications in streamflow data augmentation and forecasting. EarthArxiv, 3617. https://doi.org/10.31223/X5HM08
- Sun, A.Y., Jiang, P., Mudunuru, M.K. and Chen, X., 2021. Explore spatio-temporal learning of large sample hydrology using graph neural networks. Water Resources Research, 57(12), p.e2021WR030394.
- Tabari, H., 2020. Climate change impact on flood and extreme precipitation increases with water availability. Scientific reports, 10(1), p.13768.
- Tanir, T., Yildirim, E., Ferreira, C. M., & Demir, I. (2024). Social vulnerability and climate risk assessment for agricultural communities in the United States. *Science of The Total Environment*, 908, 168346.
- Team, G., Anil, R., Borgeaud, S., Alayrac, J.B., Yu, J., Soricut, R., Schalkwyk, J., Dai, A.M., Hauth, A., Millican, K. and Silver, D., 2023. Gemini: a family of highly capable multimodal models. arXiv preprint arXiv:2312.11805.
- Touvron, H., Martin, L., Stone, K., Albert, P., Almahairi, A., Babaei, Y., Bashlykov, N., Batra, S., Bhargava, P., Bhosale, S. and Bikel, D., 2023. Llama 2: Open foundation and fine-tuned chat models. arXiv preprint arXiv:2307.09288.
- Tran, T.D. and Kim, J., 2024. Guidance on the construction and selection of relatively simple to complex data-driven models for multi-task streamflow forecasting. Stochastic Environmental Research and Risk Assessment, 38(9), pp.3657-3675.
- UNESCO, 2023. The United Nations world water development report 2023: partnerships and cooperation for water. UN. Available at: https://unesdoc.unesco.org/ark:/48223/pf0000384655.
- Vaswani, A., Shazeer, N., Parmar, N., Uszkoreit, J., Jones, L., Gomez, A.N., Kaiser, Ł. and Polosukhin, I., 2017. Attention is all you need. Advances in neural information processing systems, 30.
- Wang, Q., Liu, Y., Yue, Q., Zheng, Y., Yao, X. and Yu, J., 2020. Impact of input filtering and architecture selection strategies on GRU runoff forecasting: A case study in the Wei River Basin, Shaanxi, China. Water, 12(12), p.3532.

- Wang, Y., Shi, L., Hu, Y., Hu, X., Song, W. and Wang, L., 2024. A comprehensive study of deep learning for soil moisture prediction. Hydrology and Earth System Sciences, 28, 917–943, https://doi.org/10.5194/hess-28-917-2024.
- Wang, L., Shi, L., Reimers, C., Wang, Y., He, L., Wang, Y., Reichstein, M. and Jiang, S., 2025. A self-supervised deep learning model for enhanced generalization in soil moisture prediction. Journal of Hydrology, p.133974.
- Ward, P.J., Jongman, B., Weiland, F.S., Bouwman, A., van Beek, R., Bierkens, M.F., Ligtvoet, W. and Winsemius, H.C., 2013. Assessing flood risk at the global scale: model setup, results, and sensitivity. Environmental research letters, 8(4), p.044019.
- Webb, M.J., Albano, C.M., Harpold, A.A., Wagner, D.M. and Wilson, A.M., 2025. Wet Antecedent Soil Moisture Increases Atmospheric River Streamflow Magnitudes Nonlinearly. Journal of Hydrometeorology, 26(6), pp.741-758.
- Wei, J., Bosma, M., Zhao, V.Y., Guu, K., Yu, A.W., Lester, B., Du, N., Dai, A.M. and Le, Q.V., 2021. Finetuned language models are zero-shot learners. arXiv preprint arXiv:2109.01652.
- Wei, J., Wang, X., Schuurmans, D., Bosma, M., Xia, F., Chi, E., Le, Q.V. and Zhou, D., 2022. Chain-of-thought prompting elicits reasoning in large language models. Advances in neural information processing systems, 35, pp.24824-24837.
- World Meteorological Organization (WMO), 2021. The Atlas of Mortality and Economic Losses from Weather, Climate and Water Extremes (1970–2019). Available at: https://library.wmo.int/idurl/4/57564.
- Xi, X., Zhuang, Q. and Liu, X., 2025. A hybrid physics-guided deep learning modeling framework for predicting surface soil moisture. Journal of Geophysical Research: Machine Learning and Computation, 2(3), p.e2025JH000682.
- Xiao, B., Wu, H., Xu, W., Dai, X., Hu, H., Lu, Y., Zeng, M., Liu, C. and Yuan, L., 2024. Florence-2: Advancing a unified representation for a variety of vision tasks. In Proceedings of the IEEE/CVF Conference on Computer Vision and Pattern Recognition (pp. 4818-4829).
- Xiang, Z., Yan, J. and Demir, I., 2020. A rainfall-runoff model with LSTM-based sequence-to-sequence learning. Water resources research, 56(1), p.e2019WR025326.
- Xiang, Z., Demir, I., Mantilla, R., & Krajewski, W. F. (2021). A regional semi-distributed streamflow model using deep learning. EarthArxiv, 2152. https://doi.org/10.31223/X5GW3V
- Xiang, Z., & Demir, I. (2022). Fully distributed rainfall-runoff modeling using spatial-temporal graph neural network. EarthArxiv, 3018. https://doi.org/10.31223/X57P74
- Xu, Y., Lin, K., Hu, C., Wang, S., Wu, Q., Zhang, L. and Ran, G., 2023. Deep transfer learning based on transformer for flood forecasting in data-sparse basins. Journal of Hydrology, 625, p.129956.
- Ye, S., Wang, J., Ran, Q., Chen, X. and Liu, L., 2021. The relative importance of antecedent soil moisture and precipitation in flood generation in the middle and lower Yangtze River basin. Hydrology and Earth System Sciences Discussions, 2021, pp.1-35.

- Zhang, Q., Yuan, Q., Jin, T., Song, M. and Sun, F., 2022. SGD-SM 2.0: an improved seamless global daily soil moisture long-term dataset from 2002 to 2022. Earth System Science Data Discussions, 2022, pp.1-22.
- Zhao, X., Wang, H., Bai, M., Xu, Y., Dong, S., Rao, H. and Ming, W., 2024. A comprehensive review of methods for hydrological forecasting based on deep learning. Water, 16(10), p.1407.
- Zuo, G., Luo, J., Wang, N., Lian, Y., & He, X. (2020). Decomposition ensemble model based on variational mode decomposition and long short-term memory for streamflow forecasting. Journal of Hydrology, 585, 124776.

Appendixes

Table A1: MAE results for the streamflow prediction task over the 7-day forecast horizon.

Day	GRU	LSTM	MambaDouble	Mamba	TransformerDouble	Transformer
1	0.519272	0.499007	0.475959	0.466031	0.500919	0.513036
2	0.690796	0.670787	0.664194	0.660749	0.682084	0.700089
3	0.785061	0.776149	0.763234	0.7797	0.787499	0.801355
4	0.850046	0.839051	0.826501	0.840934	0.848164	0.844987
5	0.89187	0.876987	0.874386	0.890233	0.888025	0.878566
6	0.930381	0.904574	0.91461	0.916307	0.917036	0.907515
7	0.956114	0.929257	0.933131	0.923491	0.942041	0.928158

Table A2: MAE results for the soil moisture prediction task over the 7-day forecast horizon.

Day	GRU	LSTM	MambaDouble	Mamba	TransformerDouble	Transformer
1	0.014559	0.013902	0.016363	0.013891	0.016442	0.015081
2	0.025903	0.02526	0.027889	0.025029	0.027513	0.025704
3	0.034916	0.034143	0.03689	0.033922	0.036428	0.034463
4	0.041654	0.04071	0.042726	0.040809	0.043187	0.040977
5	0.04666	0.045728	0.04796	0.045646	0.0485	0.046009
6	0.050704	0.049598	0.051807	0.049659	0.052756	0.050025
7	0.053951	0.052748	0.055434	0.053117	0.056185	0.053362

Table A3: RMSE results for the streamflow prediction task over the 7-day forecast horizon.

Day	GRU	LSTM	MambaDouble	Mamba	TransformerDouble	Transformer
1	1.922472	1.900571	1.800377	1.807648	1.862849	1.851881
2	2.463767	2.465472	2.430083	2.438927	2.459038	2.448385
3	2.661174	2.668327	2.641154	2.649552	2.659832	2.654145
4	2.756656	2.765681	2.745201	2.75047	2.754888	2.74901
5	2.822367	2.832587	2.812512	2.818879	2.820375	2.814732
6	2.863864	2.872902	2.860229	2.863354	2.859368	2.855115
7	2.891535	2.898194	2.888959	2.890351	2.889047	2.883534

Table A4: RMSE results for the soil moisture prediction task over the 7-day forecast horizon.

Day	GRU	LSTM	MambaDouble	Mamba	TransformerDouble	Transformer
1	0.021443	0.020748	0.023933	0.020455	0.024065	0.021857
2	0.038319	0.037837	0.040029	0.037355	0.040112	0.038029
3	0.049277	0.048871	0.0508	0.048441	0.05089	0.048751
4	0.057119	0.056705	0.058375	0.05628	0.058733	0.05646
5	0.063119	0.062733	0.06448	0.062295	0.064924	0.062473
6	0.067952	0.067523	0.069328	0.067145	0.069967	0.067353
7	0.071905	0.071456	0.073448	0.071205	0.074173	0.071464

Table A5: NRMSE results for the streamflow prediction task over the 7-day forecast horizon.

Day	GRU	LSTM	MambaDouble	Mamba	TransformerDouble	Transformer
1	1.231931	1.217897	1.153692	1.158351	1.193724	1.186696
2	1.578847	1.57994	1.557262	1.56293	1.575817	1.56899
3	1.705871	1.710456	1.693038	1.698421	1.705011	1.701365
4	1.768059	1.773847	1.760712	1.764091	1.766925	1.763155
5	1.810196	1.816751	1.803875	1.807959	1.808918	1.805299
6	1.836676	1.842472	1.834345	1.836349	1.833793	1.831065
7	1.854636	1.858907	1.852984	1.853877	1.853041	1.849505

Table A6: NRMSE results for the soil moisture prediction task over the 7-day forecast horizon.

Day	GRU	LSTM	MambaDouble	Mamba	TransformerDouble	Transformer
1	0.015994	0.015476	0.017852	0.015257	0.01795	0.016303
2	0.028582	0.028223	0.029857	0.027863	0.029919	0.028365
3	0.036755	0.036452	0.037891	0.036131	0.037958	0.036363
4	0.042604	0.042296	0.043541	0.041979	0.043808	0.042113
5	0.047079	0.046791	0.048094	0.046464	0.048425	0.046597
6	0.050683	0.050364	0.05171	0.050081	0.052186	0.050236
7	0.053632	0.053296	0.054782	0.053109	0.055323	0.053302

Table A7: Pearson's r results for the streamflow prediction task over the 7-day forecast horizon.

Day	GRU	LSTM	MambaDouble	Mamba	TransformerDouble	Transformer
1	0.858311	0.861249	0.876602	0.875818	0.868109	0.86937
2	0.752403	0.751809	0.760205	0.758599	0.753623	0.7566
3	0.701842	0.699623	0.707232	0.705151	0.70219	0.704379
4	0.672671	0.669941	0.676235	0.674541	0.673329	0.675611
5	0.652492	0.649329	0.655722	0.65356	0.653276	0.65553
6	0.639257	0.63641	0.640597	0.639618	0.640882	0.642826
7	0.630044	0.628134	0.630997	0.631018	0.630959	0.633183

Table A8: Pearson's r results for the soil moisture prediction task over the 7-day forecast horizon.

Day	GRU	LSTM	MambaDouble	Mamba	TransformerDouble	Transformer
1	0.998119	0.998173	0.997587	0.998269	0.997602	0.99804
2	0.993815	0.993913	0.993223	0.994084	0.993189	0.99391
3	0.989689	0.989821	0.989075	0.990032	0.988987	0.989935
4	0.986115	0.986271	0.985446	0.986507	0.98532	0.986458
5	0.982995	0.983169	0.98222	0.98341	0.982065	0.983383
6	0.98027	0.980477	0.979403	0.980693	0.97917	0.98065
7	0.977879	0.978114	0.97688	0.978304	0.976545	0.978181

Table A9: MASE results for the streamflow prediction task over the 7-day forecast horizon.

Day	GRU	LSTM	MambaDouble	Mamba	TransformerDouble	Transformer
1	1.070802	1.029013	0.981485	0.961013	1.032957	1.057943
2	1.424847	1.383576	1.369977	1.362872	1.406878	1.444016
3	1.619147	1.600766	1.574129	1.60809	1.624175	1.652752
4	1.757937	1.735199	1.709245	1.739094	1.754045	1.747475
5	1.844635	1.813852	1.808473	1.841248	1.836682	1.817118
6	1.924021	1.870652	1.891406	1.894916	1.896423	1.876733
7	1.977345	1.921801	1.929813	1.909876	1.948239	1.919529

Table A10: MASE results for the soil moisture prediction task over the 7-day forecast horizon.

Day	GRU	LSTM	MambaDouble	Mamba	TransformerDouble	Transformer
1	0.800976	0.764849	0.900237	0.764247	0.904566	0.829719
2	1.425039	1.389627	1.534272	1.376931	1.513589	1.414074
3	1.920755	1.878257	2.029341	1.8661	2.003942	1.895833
4	2.291181	2.239287	2.350156	2.244729	2.375524	2.253975
5	2.565922	2.514677	2.637401	2.510161	2.667111	2.53013
6	2.788222	2.727385	2.848904	2.730749	2.901079	2.750909
7	2.9673	2.901101	3.048883	2.921395	3.09014	2.9349

Table A11: Spearman's p results for the streamflow prediction over the 7-day forecast horizon.

Day	GRU	LSTM	MambaDouble	Mamba	TransformerDouble	Transformer
1	0.910781	0.910788	0.911947	0.922862	0.934267	0.941543
2	0.897668	0.903687	0.891105	0.902568	0.918479	0.920182
3	0.887819	0.894096	0.878252	0.887966	0.902981	0.905148
4	0.8784	0.887624	0.872375	0.880773	0.891451	0.894535
5	0.871128	0.878721	0.868141	0.873644	0.882598	0.885987
6	0.861786	0.87561	0.858416	0.869048	0.875639	0.879304
7	0.852506	0.869607	0.851783	0.863046	0.870043	0.873783

Table A12: Spearman's p results results for the soil moisture prediction over the 7-day forecast horizon.

Day	GRU	LSTM	MambaDouble	Mamba	TransformerDouble	Transformer
1	0.998	0.998047	0.997492	0.998172	0.997557	0.997875
2	0.993314	0.993393	0.9927	0.99358	0.992635	0.993358
3	0.98881	0.988922	0.988168	0.989142	0.988025	0.989013
4	0.984924	0.985063	0.984225	0.985279	0.984027	0.985226
5	0.981555	0.981719	0.980736	0.981913	0.980502	0.981895
6	0.978626	0.97883	0.977691	0.978998	0.977379	0.978941
7	0.976062	0.976298	0.974966	0.976445	0.97454	0.976269

Table A13: Taylor Skills Scores for the streamflow prediction over the 7-day forecast horizon.

Day	GRU	LSTM	MambaDouble	Mamba	TransformerDouble	Transformer
1	0.7185	0.729761	0.760636	0.753574	0.735967	0.749941
2	0.534986	0.538947	0.55227	0.541369	0.539423	0.556366
3	0.454005	0.45859	0.472053	0.457032	0.45929	0.476966
4	0.414771	0.417377	0.424536	0.417841	0.417198	0.430137
5	0.387775	0.388312	0.392329	0.390207	0.389073	0.398778
6	0.368623	0.371933	0.379226	0.364723	0.371386	0.381588
7	0.355078	0.366275	0.361267	0.34955	0.358198	0.366429

Table A14: Taylor Skills Scores for the soil moisture prediction over the 7-day forecast horizon.

Day	GRU	LSTM	MambaDouble	Mamba	TransformerDouble	Transformer
1	0.996047	0.996349	0.995119	0.996534	0.995025	0.995899
2	0.987375	0.987872	0.986337	0.988218	0.986188	0.98757
3	0.979161	0.979746	0.97794	0.980203	0.977748	0.979547
4	0.971979	0.972716	0.97088	0.973107	0.970255	0.972533
5	0.965826	0.966581	0.964454	0.966949	0.963505	0.966341
6	0.96035	0.961315	0.959063	0.961498	0.957464	0.960849
7	0.955572	0.956708	0.953803	0.956883	0.952147	0.955887